Accuracy of GFS Forecasts: An Examination of High-Impact 2011–2012 Cold Season Weather Events

DANIEL F. DIAZ[1, 2], STEVEN M. CAVALLO[3], and BRIAN H. FIEDLER[3]

[1]National Weather Center Research Experiences for Undergraduates Program, Norman, Oklahoma
and
[2]The Florida State University, Tallahassee, FL

[3]School of Meteorology, The University of Oklahoma, Norman, Oklahoma

ABSTRACT

Numerical weather prediction models are thought to handle certain situations with a diminished level of skill, such as with baroclinic Rossby wave packets in the midlatitudes and with large-scale regime changes associated with the onset of atmospheric blocking. Using analysis and forecast data from the NCEP GFS model, this study examines the forecast skill of the 2011–2012 cold season in the Northern Hemisphere with the hypothesis that relatively large model error is primarily associated with baroclinic Rossby wave packets and the onset of atmospheric blocking events. Forecast skill is diagnosed by examining forecast model error through the use of Hovmöller diagrams and the 500 hPa geopotential height anomaly correlation skill score. These diagnostics identify cases which exhibit relatively large error in the forecast model, including tropopause-level wave packets and associated forecast error at the surface. One such event, a 955 hPa surface low, is examined in detail during November 2011, which is found to be associated with relatively large error downstream at later times. Although there are some instances of increased model error in wave packets, coherent patterns of error are not present with every wave packet identified in this study. Additionally, the onset of a long-lived blocking ridge of high pressure around 20° E longitude, which persisted intermittently from the middle of October 2011 to March 2012, is examined. This ridge is found to become stationary after a series of breaking baroclinic Rossby waves impact it, and low skill is seen during its transition from a non-stationary to a stationary ridge. However, no definitive conclusions can be made regarding the source or characteristics of model error for this particular event, and further examination is necessary to gain a better understanding of this event.

1. INTRODUCTION

Situations exist in which numerical weather prediction models perform with a diminished skill. Error apparent in models, which include The National Center for Environmental Prediction (NCEP) Global Forecast System (GFS) model and the European Centre for Medium-Range Weather Forecasts (ECMWF), has been studied in cases of tropical cyclone and extratropical transition positions (Buckingham et al. 2010), extratropical cyclones in the northern Pacific and Bering Strait (Colle and Charles 2011), and in the onset of atmospheric blocking (Tibaldi and Molteni 1990). Studies by Hakim (2003) and Chang (2005) have shown how forecast error can propagate with wave packets across the Pacific Ocean.

Given the above, we expect that the models lose skill with the presence of wake packets in the midlatitudes. The GFS model is chosen for this study because it is NCEP's operational model and its archived data is freely available (Global Climate and Weather Modeling Branch 2003).

This study, motivated by high impact weather events of the 2011–2012 Northern Hemisphere cold season, makes an effort to correlate those events to wave packets that exist in the midlatitudes and examine the error associated with forecasts of the wave packets or the associated weather events. The term 'wave packet' is used in reference to a succession of baroclinic Rossby waves on a global scale. The wave packet propagates with a distinct group velocity, while the individual disturbances within the packet propagate at an independent phase speed. The individual disturbances, or eddies, grow and decay within the packet, and their phase speed is slower than that of the group velocity (Lee and Held 1993). Surface cyclones develop in

[1] *Corresponding author address:* Daniel Frank Diaz, National Weather Center Research Experiences for Undergraduates Program, 1400 W. Tharpe Street, Tallahassee, FL, 32303. E-mail: dfd09@my.fsu.edu

association with upper-level potential vorticity anomalies, which are embedded in Rossby wave packets; this is one case in which the accurate prediction of wave packets implies the accurate prediction of weather at the surface. Downstream development of ridges, troughs, and cyclones can occur as a result of upstream disturbances within a wave packet (Hakim 2003). Understanding the characteristics of wave packets is important in order to understand model error characteristics (Zimin et al. 2003).

In this project, we examine the characteristics of model error during the 2011–2012 Northern Hemisphere cold season. We hypothesize that relatively high model error is associated with particular events, such as an extratropical cyclone that impacted the western coast of Alaska in November 2011 and the onset of an anticyclonic blocking pattern in October 2011. Furthermore, we expect that both events are associated with Rossby wave packets.

Methods employed in this study are outlined in section 2 and the results are described in section 3. Speculations of results that were not proven within the scope of this study are presented in section 4, and a synopsis of the project, as well as potential improvements are given in section 5.

2. METHODS

a. Event recognition

Hovmöller diagrams are chosen as a concise way to identify and quantify forecast error. Unless otherwise noted, all Hovmöller diagrams described in this manuscript depict an average of the plotted parameter from 30° to 60° N latitude, using gridded 0.5° GFS data for all longitudes. The plotted times on each diagram are either the analysis or the forecast valid at 0000 UTC and 1200 UTC for each day represented. When a required analysis or forecast record is empty or is missing the necessary parameter, the record is substituted with the next available forecast valid at the required time. This method is the best way to maintain continuity among the Hovmöller diagrams, ensuring that data is plotted at an even twelve-hour time interval throughout the month represented in a given diagram. See APPENDIX for a list of missing records and the forecasts used to replace them. Hovmöller diagrams are produced from the GFS analysis data and for each forecast time at 24 hour intervals, up to 144 hours.

The mean spatial and temporal locations of the wave packets are introduced by plotting Hovmöller diagrams of the meridional component of wind at the tropopause level. The meridional component of wind is chosen because it depicts a deviation from a zonal jet, which is indicative of waves. The expectation is that a relationship is found between these wave packets and the events of interest.

Hovmöller diagrams of sea level pressure anomaly are plotted in order to identify the approximate spatial and temporal location of events that influence the weather at the surface, such as cyclogenesis. Wave packets identified at the tropopause level are visually related to surface features on the diagram, such as a deepening low pressure center or a series of developing low pressure centers downstream of the initial location. One particularly strong event, hereafter referred to as the Bering Sea storm, is of greatest initial interest, but other events that stand out to a comparable degree, or exhibit significant error will be investigated. For sea level pressure diagrams, anomalies are derived from a spatial mean at a given time. For example, at 0000 UTC on November third, the mean sea level pressure is calculated for the entire latitude circle. The anomaly is then defined as that mean, subtracted from the forecast sea level pressure at each half-degree of longitude, at that specific time. This process is executed for every plotted longitude at every plotted time.

Geopotential height at 500 hPa is plotted on Hovmöller diagrams to contribute to a more continuous representation of the atmosphere between the surface and the tropopause level. For instance, with the onset of a stationary ridge over Europe, 500 hPa heights more clearly portray changes in wave amplitude, whereas changes in the v-component of the wind on the tropopause can be relatively small. Similar to the v-component of wind at the tropopause, the 500 hPa geopotential height diagrams illustrate the wave packets that translate to that pressure level, and how they interact with or are interrupted by the block. Furthermore, 500 hPa geopotential heights are used to calculate the anomaly correlation skill scores, which will be discussed in section 2c.

As the only readily-available anomaly field from the NCEP GFS archive, the 500 hPa geopotential height anomaly field quantifies how the events of interest for this study deviate from the climatological mean state for the dates at which they take place. Using the 500 hPa geopotential height analysis data, the long-term climatological

mean can be calculated and plotted. With this mean state, the anomaly correlation is calculated later in the study.

b. Determine forecast error

To determine forecast error and plot it on a Hovmöller diagram, the operation:

$$Error = Analysis - Forecast \qquad (1)$$

is performed on every item of the arrays plotted for the analysis diagram and the diagram constructed from the forecast data for which the error is to be determined. This process is used to fashion a six-panel collection of Hovmöller diagrams for a given parameter, such as 500 hPa geopotential height, which illustrate the error apparent in each forecast at 24 hour intervals. Continuing with this example, the produced images show the difference between the analysis field of heights and the heights that were forecast at a certain lead time.

The significance of the error diagrams is to expose whether phenomena were forecast accurately in time, space, or intensity, or any combination of these measures, as well as illustrate the evolution of error with an increasing forecast lead time. A displacement error, or a disagreement between the analysis and forecast in time, space, or both, is portrayed as a paired warm- and cold-colored signature on an error diagram. Intensity errors are illustrated by a lone warm- or cold-colored signature on an error diagram, indicative of an event that was likely predicted to occur at the correct spatial location, at the correct time, but error was evident in the forecast magnitude of the event. For example: a low pressure center that was not forecast as deep as was indicated by the GFS analysis.

c. The anomaly correlation

The anomaly correlation (AC), based on the equation by Wilks (1995), is defined here as:

$$AC = \frac{\overline{(f-c)(a-c)}}{\sqrt{\overline{(f-c)^2}\ \overline{(a-c)^2}}}, \qquad (2)$$

and is used to provide a quantitative measure for describing forecast error evident in the Hovmöller diagrams. It furnishes a basis of comparison for errors associated with the different features under study. The AC was designed to quantify the strength of the correlation between the forecast anomaly and the observed anomaly. Possible values for the AC range from 0 to 1. An AC of 0 means there is no correlation, and an AC of 1 corresponds to a perfect correlation.

The AC is calculated for each forecast (24 hr, 48 hr, 72 hr, 96 hr, 120 hr, and 144 hr), for each time plotted on a Hovmöller diagram. A time series of the AC is plotted for October 2011 and November 2011. Local minima on the time series are intended to reveal specific instances in which the model performed with the lowest skill.

3. RESULTS

a. Blocking ridge over Europe

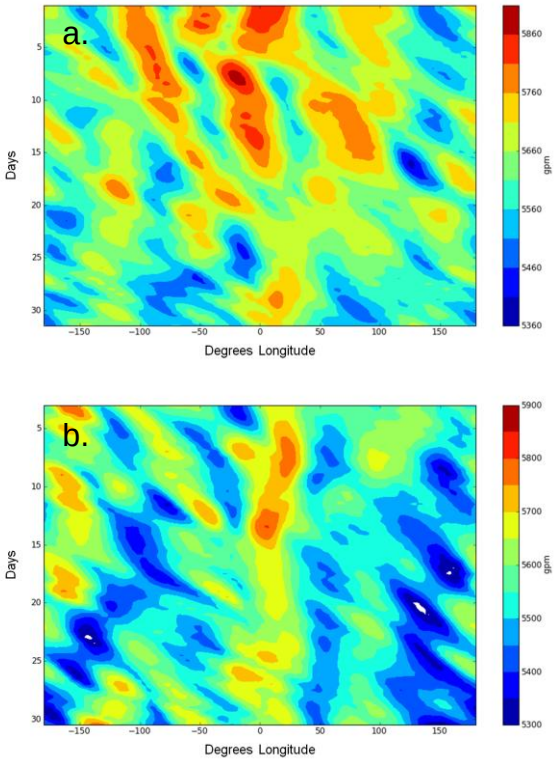

FIG. 1. Hovmöller diagrams of 500 hPa geopotential height averaged over 30° to 60° N for (a) October 2011 and (b) November 2011. The onset of a blocking ridge at 20° E is characterized by relatively higher heights of the pressure surface on 26 October 2011. The block is shown here to persist though November 2011.

The onset of the blocking ridge over Europe is indicated by a rise in 500 hPa geopotential height at approximately 20° E on 26 October 2011 (Fig. 1). A wave packet, identifiable at the 500 hPa level in Figure 1 and at the dynamic tropopause in Figure 2, can be traced on these Hovmöller diagrams from 120° W on 5 October 2011 until it

terminates, or stops propagating, at 20° E on 26 October 2011 as the stationary ridge. This block deamplifies and propagates downstream after persisting through the month of November before a stationary ridge sets up over the same region again in January and February 2012.

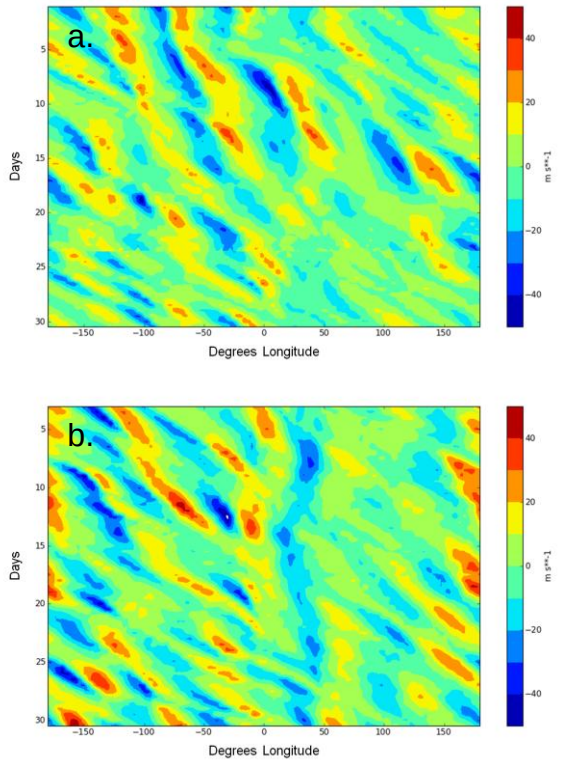

FIG. 2. Hovmöller diagrams of the meridional component of wind at the tropopause, averaged over 30° to 60° N for (a) October 2011 and (b) November 2011. Wave packets exist upstream of the blocking ridge (centered at 20° E) during October and November.

In general, most of the error apparent with waves in the upper atmosphere at any lead time under evaluation for October or November precedes the blocking ridge. This is visually evident in Figures 3 and 4, which show the forecast error for the meridional component of wind at the tropopause during the months of October and November 2011. The same is true with the error in forecasts of 500 hPa geopotential height. There is more error upstream of the block, where wave packets are evident, than there is downstream of the block. The evolution of forecast error in time can also be seen in the Hovmöller diagrams. When examining the plots of the meridional component of wind at the tropopause for October and November, the 24- and 48-hour forecasts exhibit nearly no error greater than a magnitude of 10 m s^{-1}. In Figures 3 and 4, which show forecast error at the 96-, 120- and 144-hour lead times, error is observed over an increasing area and at greater magnitudes as the lead time increases.

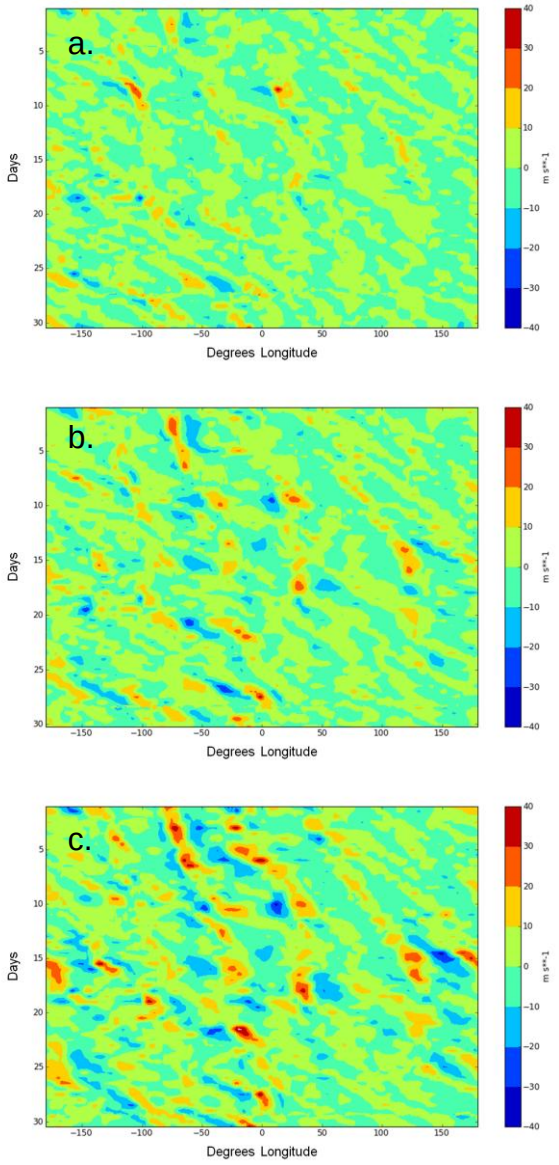

FIG. 3. Hovmöller diagrams illustrating GFS forecast error for the meridional component of wind at the tropopause at lead times of (a) 96, (b) 120, and (c) 144 hours for October 2011. Less error exists downstream of the blocking ridge after it becomes stationary.

Blocking of this nature is known to be handled with difficulty by the ECMWF model, and medium-range forecast models in general (Pelly and Hoskins 2003). However, the block onset, identified around 26 October 2011, has relatively low

forecast error compared to other features on both the meridional wind and the 500 hPa geopotential height diagrams.

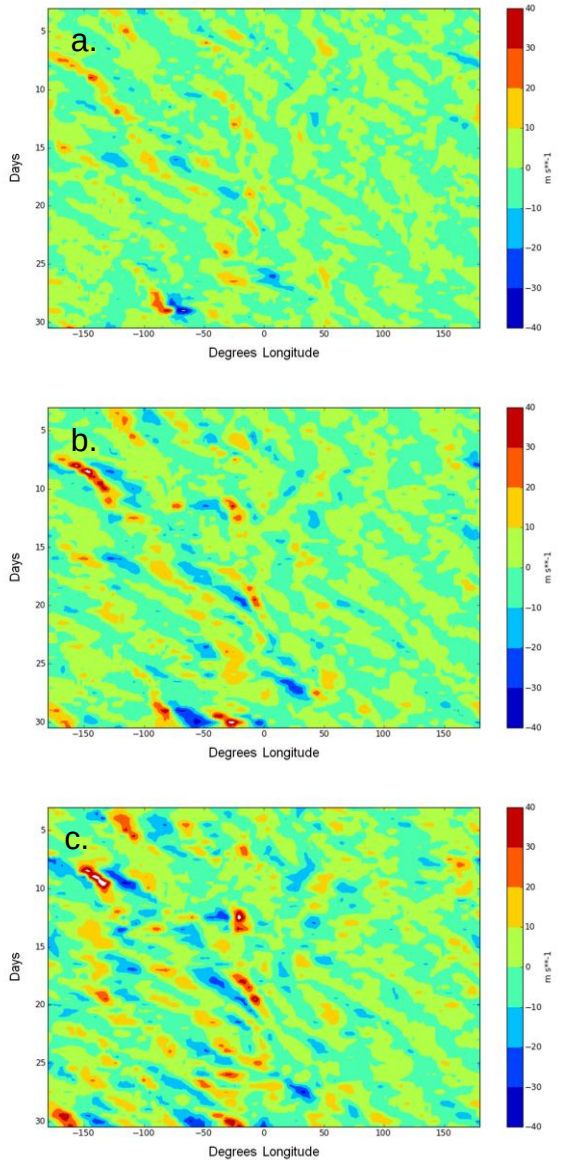

FIG. 4. Hovmöller diagrams illustrating GFS forecast error for the meridional component of wind at the tropopause at lead times of (a) 96, (b) 120, and (c) 144 hours for October 2011. There are fewer error signatures downstream of the blocking ridge (20° E) than there are upstream of the ridge.

b. Extratropical cyclone in the North Pacific Ocean

An area of low pressure (circled in Fig. 5) initiates at 150° E on 6 November 2011 and tracks north-eastward along with a wave packet at the upper levels across the Pacific Ocean towards the Bering Sea. This cyclonic storm is not well forecast beyond 96 hours, which is evidenced by the error signatures circled in Figure 6b and 6c. The 24-, 48-, and 72-hour forecasts for the mean surface pressure anomaly associated with this storm exhibit nearly no error greater than a magnitude of 5 hPa. It is no coincidence that the

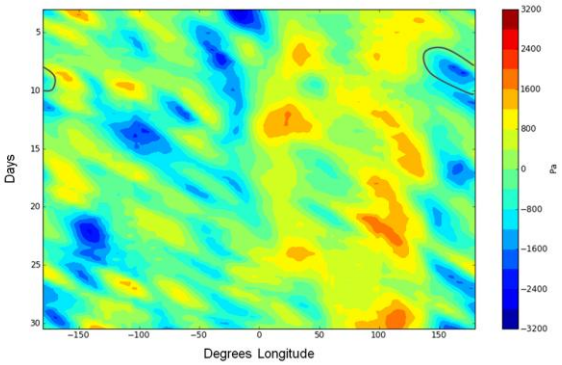

FIG. 5. Hovmöller diagram of the mean sea level pressure anomaly (see definition of anomaly in METHODS), averaged over 30° to 60° N. The low pressure anomaly, deepest at 160° E on 8 November 2011, represents a cyclonic storm that tracked across the Pacific Ocean before impacting the western coast of Alaska.

wave packet reflected in the meridional wind pattern initiates at the same time off the southeast coast of Japan. The conditions that exist with the upstream edge of that Pacific wave packet (Fig. 2b.) provide an ideal situation for cyclogenesis (Hakim 2003). Both the cyclone that developed off the coast of Japan and the associated wave packet were handled well by the forecast model until the 96-hour forecast, when error appears among both features (compare Fig 6a,b,c and Fig 4a,b,c).

c. Patterns of error

Among all the fields plotted in the Hovmöller diagrams of this study, it is important to note that, although error in the shorter-term forecasts was low in comparison to the error apparent in the longer-term forecasts under examination, it is not the case that there was no error in these short term forecasts. If the error is instead normalized by its standard deviation, error would be revealed in more areas on the short-term diagrams. However, although more error signatures would be present among the shorter lead times, such as 24 and 48 hours, these errors are smaller in magnitude in comparison to the error at greater lead

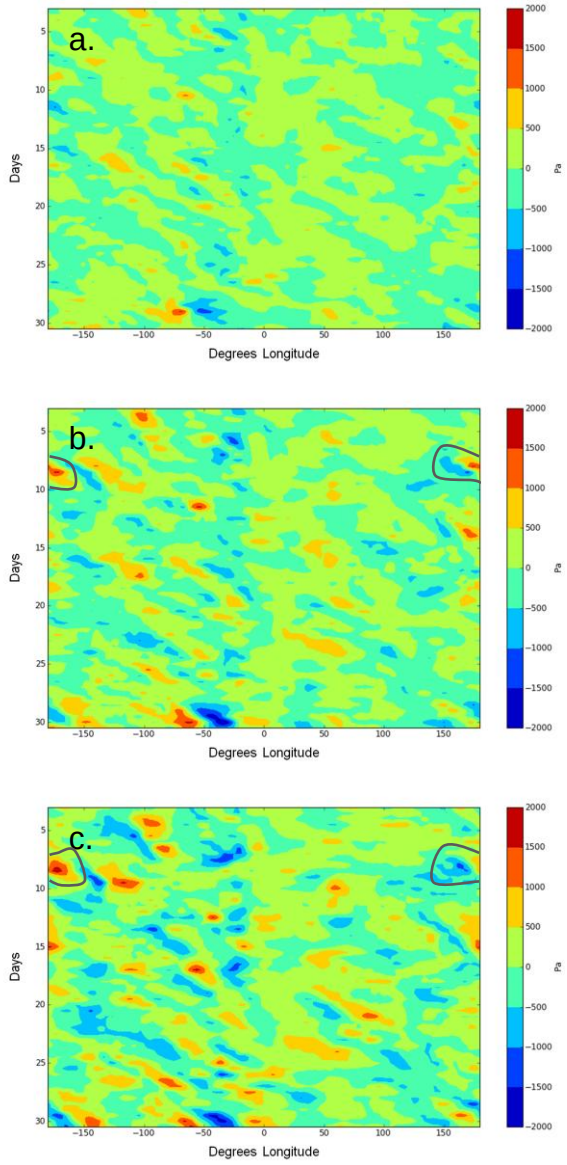

FIG. 6. Hovmöller diagrams illustrating GFS forecast error associated with the mean sea level pressure anomaly predicted at lead times of (a) 96, (b) 120, and (c) 144 hours for November 2011.

times, and they are more random. If we assume a normal distribution of error, when the standard error is plotted on a Hovmöller diagram, it becomes evident that error is less random and follows a more coherent pattern as the forecast lead time increases. For example, consider the standard error of the meridional component of wind at the tropopause for October 2011 at the 24- and 144-hour forecast times. The 24-hour Hovmöller diagram exhibits many signatures greater than two standard deviations, scattered randomly over the area of the plot for the month. However, these errors are frequent, and do not noticeably correspond with any organized feature of the meridional component of wind at the tropopause. In contrast, the standard error plotted on a Hovmöller diagram for the 144 hour forecast shows an error pattern similar to that shown in Figure 4c, which is a more coherent pattern that reflects the pattern of waves on the tropopause. This emphasizes the statistical significance of the forecast error associated with the wave packets preceding the onset of the block.

d. Anomaly correlation

The AC score, given by equation (2), provides a quantitative basis for the comparison of errors at specific times. A general observation is that the observed anomaly and the forecast anomaly have a stronger correlation at shorter lead times. Regardless of the lead time under consideration, the times indicated by local minima in the AC time series (Fig. 7) are consistent among each lead time, within a range of three days.

The most significant AC minima in the month of October 2011 occur at 0000 UTC on 18 October 2011 ±24 hours. When examining the mean 500 hPa heights between 30° and 60° N at the future location of the block over Europe (20° E), one is able to identify a ridge that has been steadily moving east until that time at approximately that location. Evident in the meridional component of wind at the tropopause, that ridge was part of a wave packet that traversed all longitudes before a different, final ridge on the leading (easternmost) edge of that wave packet ceases its forward propagation and becomes the stationary block on 26 October 2011. However, this single ridge is not the only feature to exhibit error at this date. Error is evident at locations spaced intermittently across all longitudes on approximately 18 October 2011 (most visibly evident in Figure 3d). The reason for this error is beyond the scope of the present study, and may perhaps best be examined in a numerical modeling study. Possible features of interest here are the sensitivity to model initial conditions, stratospheric-tropospheric connections, and air-ocean-sea ice interactions, as this event occurred in part over a region of strong air-sea temperature gradients. However, it is clear that those errors do not directly reflect a coherent wave packet which would propagate forward in time.

During November 2011, wave packets occur throughout the month, upstream of the blocking

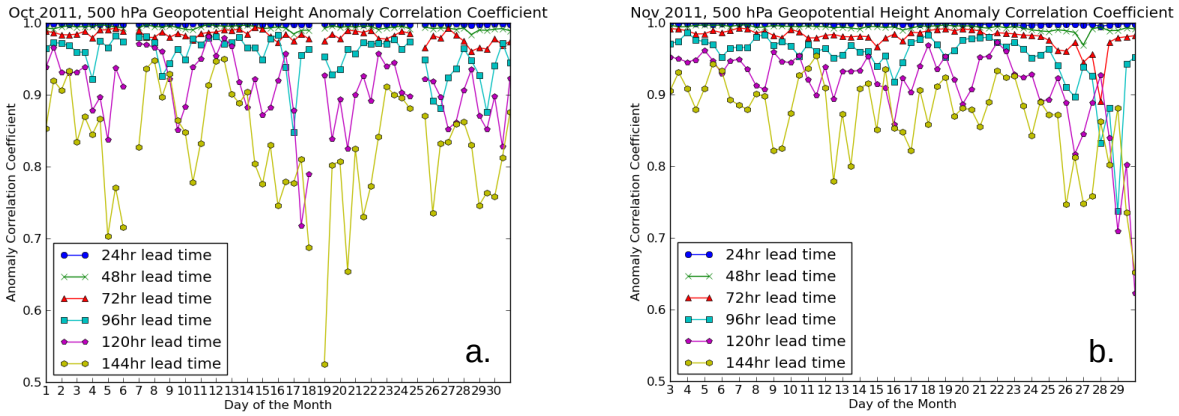

FIG. 7. Time series of the anomaly correlation of 500 hPa geopotential height for all GFS forecast lead times for (a) October 2011 and (b) November 2011. Minima in the anomaly correlation are evident on approximately 18 October 2011 and 28 November 2011.

ridge over Europe. In some instances, a pattern of error is reflected in the individual waves of that wave packet. Contrary to what was expected, the errors associated with these wave packets do not exhibit the poorest ACs for that month, and not every wave packet is associated with a coherent pattern of error. The poorest AC for November occurs at 1200 UTC on 28 November 2011 ±36 hours. At 500 hPa, this isolated error event is associated with a single ridge axis over the continental United States (see Fig. 6 with the error signature centered at 60° W on 29 October 2011). This ridge appears to be part of a wave packet, identifiable at the 500 hPa level and at the tropopause. Here, error is not evident in the wave pattern as is seen in other cases. The error is restricted to that single trough/ridge placement in time.

4. DISCUSSION

The final ridge that propagated eastward to the location of the block over Europe exhibits error in the GFS forecasts at the greater lead times under examination on approximately 18 October 2011, when it ceases its forward propagation. This is evidenced by the AC minima (Fig. 7) and the forecast error Hovmöller diagrams for October. In contrast, the blocking pattern showed comparatively low error in its persisting form. When considering initial conditions as a source of error, this statement may not hold true if we were to examine greater lead times. In this case, the block onset was preceded by a series of anticyclonic wave breaking events. In this study, which only encompasses lead times up to 144 hours, the last wave packet that led into the block was present, even if handled with some degree of error, at all lead times examined. During November 2011, relatively no error is seen with the placement of the persisting block. However, in this study, the earliest forecast, valid for 1 November 2011 was only initialized 144 hours, or 6 days, before that valid time. Consider that 6 days before 1 November 2011, the blocking ridge was already in place, and that final wave break had already occurred. With that, if we were to examine forecasts of lead times greater than 144 hours, it is speculated that the model skill would be significantly degraded in the forecast of the persisting block at the very end of October 2011 and throughout November 2011. The extent of this study shows that the block onset was handled with poor skill, but once the block was in place, the model performed well.

Concerning the extratropical cyclone that impacted the western coast of Alaska, error was evident in the spatial and temporal placement of the cyclone and the wave packet at upper levels. It appears that each trough and ridge of the wave packet (first evident when the cyclone develops) over the Pacific Ocean, which leads in to the block over Europe, was offset slightly in space and time, especially in the longer-term forecasts. The propagation of error with this wave packet at the tropopause can be visually traced on Figure 4c from 160° E on 8 Nov 2011 to 30° W on 13 Nov 2011. Positive and negative errors in the sea level pressure anomaly reflect this pattern at the surface (Fig. 6c). We can infer that the model's timing and location of the surface low was impacted by the error in the upper-level wave packet.

5. CONCLUSIONS

a. Summary

This study examined the GFS model error characteristics of the 2011-2012 Northern Hemisphere cold season. Motivated by select high-impact weather events, such as a blocking ridge over Europe in October 2011 and the Bering Sea storm in November 2011, it was hypothesized that model error increases in association with wave packets and large-scale regime changes. Error was found in this study to be relatively large among wave packets in the upper atmosphere that were associated with these two events for forecast lead times greater than approximately 72 hours. However, other wave packets of comparable magnitudes were identified that were not associated with similar degradation of model skill.

Among the 24–144-hour forecast lead times under examination, model skill was degraded with the block onset. However, once the block was in place, the model exhibited little error in its spatial placement. Regarding the extratropical cyclone that impacted Alaska, error with a wave packet at upper levels seemed to imply error in the event forecast at the surface. The Bering Sea storm developed in the upstream edge of the wave packet, and a succession of error in the mean sea level anomaly progressed downstream along with the waves overhead. Successive positive and negative errors in the forecast mean sea level pressure anomaly appear between 150° E on 6 November 2011 and 0° on 13 November 2011, which is approximately the location of the block at upper levels. Due to the observation that more error was evident before the block onset occurred and upstream of the block once it was in place at all levels examined, we conclude that there is a correlation between degradation of model skill and the presence of a wave packet. In other words, where there were no wave packets present, the model performed with higher skill. However, it is not the case that every wave packet identified in this study had a coherent pattern of error associated with it. The Anomaly Correlation at each date supports this point by revealing that the poorest correlation between observed anomalies and forecast anomalies for the 500 hPa geopotential height were not necessarily associated with a wave packet.

This is not the first study to use the anomaly correlation score as a measure of forecast skill. In a study by Jones et al. (2003), the AC for 500 hPa geopotential height forecasts is used to identify a degradation of forecast skill corresponding to cases of extratropical transition. The transitioning tropical cyclones cause distinct minima in the AC time series, similar to the minima that we use to identify instances of decreased skill with the GFS model. Jones also notes that the magnitude of the decrease of skill for the NOGAPS model becomes larger with an increase in forecast interval. The same finding is shown in this study, with forecast lead times from 24 to 144 hours.

There is not enough evidence here to prove the hypothesis that the highest errors are always spatially and temporally correlated with wave packets and the onset of the blocking ridge. However, this work is significant because it is generally accepted that models do not perform well under these conditions. The GFS model is a common tool for forecasters in the operational environment, and it is important to identify specific instances where the model had trouble, as well as events where the model handled these events comparatively well. More work remains to be done to determine why the model performed well in some of these cases but not others.

b. Improvements and future work

To enhance the quality of this work, a statistical analysis must be performed to qualitatively define a significant error. Additionally, all conclusions drawn here are based on the identification of absolute error. The absolute error downstream of the block was small in comparison to the absolute error upstream of the block. However, it is not to say that there was no error downstream of the block. The relative error downstream of the block needs to be considered with respect to the field that exists in that downstream region. If significant error exists in that region, an additional investigation may be inspired to determine the source of those errors.

To establish statistical significance, more cases of cyclogenesis, block onset, and wave patterns in general need to be examined under the conditions present for the events examined in this study. Even with the cases that are present in this study, further investigation must be done to determine the dynamics behind these events and to answer questions such as: Why did one wave packet exhibit coherent error propagating along with it, while others did not?

Adding greater forecast lead times to the study will allow us to determine whether some of the apparent errors that have already been identified are due to changes in initial conditions for the different model runs.

6. ACKNOWLEDGMENTS

This material is based upon work supported by the National Science Foundation under Grant No. AGS-1062932.

The statements, findings, conclusions, and recommendations are those of the authors and do not necessarily reflect the views of the National Science Foundation.

8. APPENDIX

The following is a list of empty GFS records, the valid date and time for each, and the last eleven characters of the filename of the .grb2 files used in place of each missing record required for this study.

These records are available online at: ftp:// nomads.ncdc.noaa.gov/GFS/Grid4/

DATE MISSING:	VALID ON: date:	time:	SUBSTITUTED WITH:
gfsfore000:			
10/12	10/12	1200	12_0600_006
10/13	10/13	0000	12_1200_012
10/17	10/17	0000	16_0000_024
		1200	17_0000_012
10/1	10/18	0000	17_0000_024
		1200	18_0600_006
10/19	10/19	0000	18_1800_006
		1200	19_0000_012
10/20	10/20	1200	20_0000_012
10/24	10/24	0000	23_1800_006
10/25	10/25	0000	24_1800_006
		1200	25_0000_012
gfsfore024:			
10/12	10/13	0000	12_0600_018
		1200	12_1800_018
10/17	10/18	1200	17_1800_018
10/18	10/19	0000	18_0600_018
		1200	18_1800_018
10/19	10/20	0000	19_0600_018
10/21	10/22	0000	21_1200_012
10/24	10/25	0000	24_0600_018
gfsfore048:			
10/16	10/18	1200	16_1800_042
10/17	10/19	1200	17_1800_042
10/25	10/27	1200	25_0600_054
10/26	10/28	0000	26_0600_042
		1200	26_0000_060
gfsfore72:			
10/12	10/15	0000	12_0600_066
10/18	10/21	0000	18_0600_066
10/19	10/22	1200	19_0600_078
10/21	10/24	1200	21_1800_066
10/23	10/26	0000	23_0600_066
10/26	10/29	1200	26_0600_078
gfsfore96:			
10/17	10/21	1200	17_0600_102
10/18	10/22	0000	18_0600_090
10/20	10/24	0000	20_0600_090
	10/24	1200	20_1800_090
10/21	10/25	0000	20_1800_102
10/22	10/26	0000	22_0600_090
10/24	10/28	0000	24_0600_090
10/25	10/29	0000	25_1200_084
10/26	10/30	1200	27_0000_084
10/27	10/31	1200	27_0600_102
gfsfore120:			
10/19	10/24	1200	19_0600_126
10/24	10/29	0000	24_0600_114
10/26	10/31	1200	25_1200_144
gfsfore144:			
10/12	10/18	0000	12_0600_138
10/17	10/23	1200	17_0600_150
10/19	10/25	0000	19_0600_138
10/24	10/30	0000	24_0600_138

REFERENCES

Buckingham, C., T. Marchok, I. Ginis, L. Rothstein, and D. Rowe, 2010: Short- and medium-range prediction of tropical and transitioning cyclone tracks within the NCEP Global Ensemble Forecasting System. *Wea. Forecasting,* **25**, 1736–1754.

Chang, E. K. M., 2005: The impact of wave packets propagating across Asia on Pacific cyclone development. *Mon. Wea. Rev*., **133**, 1998–2015.

Colle, B. A., and M. E. Charles, 2011: Spatial distribution and evolution of extratropical cyclone error over North America and its adjacent oceans in the NCEP Global Forecast System model. *Wea. Forecasting,* **26***,*129– 149.

Global Climate and Weather Modeling Branch, EMC, 2003: The GFS atmospheric model. Tech. rep., NCEP Office Note 442, 14 pp. [Available online at http://www.emc.ncep.noaa.gov/office notes /newernotes/on442.pdf]

Hakim, G. J., 2003: Developing wave packets in the North Pacific storm track. *Mon. Wea. Rev*., **131**, 2824–2837.

Jones, S. C., P. A. Harr, J. Abraham, L. F. Bosart, P. J. Bowyer, J. L. Evans, D. E. Hanley, B. N. Hanstrum, R. E. Hart, F. Lalaurette, M. R. Sinclair, R. K. Smith, and C. Thorncroft, 2003: The extratropical transition of tropical cyclones:

forecast challenges, current understanding, and future directions. *Wea. Forecasting,* **18**,1052–1092.

Lee, S., and I. M. Held, 1993: Baroclinic wave packets in models and observations. *J. Atmos. Sci.,* **50**, 1413–1428.

Pelly J. L., and B. J. Hoskins, 2003: How well does the ECMWF ensemble prediction system predict blocking?. *Q. J. R. Meteorol. Soc.*, **129**, 1683–1702.

Tibaldi, S., and F. Molteni, 1990: On the operational predictability of blocking. Tellus, **42A**, 343–365.

Wilks, D. S., 1995: *International Geophysics Series.* Vol. 59, Academic Press, 467 pp.

Zimin, A. V., I. Szunyogh, D.J. Patil, B.R. Hunt, and E. Ott, 2003: Extracting Envelopes of Rossby Wave Packets. *Mon. Wea. Rev.*, **131**, 1011–1017.